Original Article

Iron metabolism regulation of epithelial-mesenchymal transition in idiopathic pulmonary fibrosis

Yi Han[1#], Ling Ye[2#], Fang Du[3#], Maosong Ye[2], Chun Li[2], Xiaodan Zhu[2], Qin Wang[2], Hongni Jiang[2], Zilong Liu[2], Jiefei Ma[4], Jian Zhou[2], Chunxue Bai[2], Yuanlin Song[2], Jie Liu[2]^

[1]Department of Emergency Medicine, Zhongshan Hospital, Fudan University, Shanghai, China; [2]Department of Pulmonary and Critical Care Medicine, Zhongshan Hospital, Fudan University, Shanghai, China; [3]Department of Anesthesia, Zhongshan Hospital, Fudan University, Shanghai, China; [4]Department of Critical Care Medicine, Zhongshan Hospital, Fudan University, Shanghai, China

Contributions: (I) Conception and design: J Liu, Y Han; (II) Administrative support: Y Song, C Bai; (III) Provision of study materials or patients: J Liu, Y Han, L Ye, F Du; (IV) Collection and assembly of data: Y Han, L Ye, X Zhu, Q Wang, Z Liu, J Ma; (V) Data analysis and interpretation: J Liu, F Du, M Ye, C Li, H Jiang, J Zhou, Y Song; (VI) Manuscript writing: All authors; (VII) Final approval of manuscript: All authors.

[#]These authors contributed equally to this work.

Correspondence to: Jie Liu; Yuanlin Song. Department of Pulmonary and Critical Care Medicine, Zhongshan Hospital, Fudan University, Shanghai 200032, China. Email: liu.jie2@zs-hospital.sh.cn; song.yuanlin@zs-hospital.sh.cn.

Background: Iron overload has been found in the lungs of patients with idiopathic pulmonary fibrosis (IPF) and is thought to be involved in disease progression; however, the underlying mechanism is complex and not yet fully understood. We sought to assess the *in vitro* role of iron in the progression of fibrosis in lung epithelial cells, and examine the possible regulation of iron and IPF.

Methods: Erastin was used to establish a cell model of iron accumulation in mouse lung epithelial cell line 12 (MLE-12). A Cell Counting Kit-8 assay and annexin V staining were applied to measure cell viability and apoptosis, quantitative polymerase chain reaction (qPCR) and quantitative immunoblot analysis of the protein was conducted to analyze the expression of E-cadherin, N-cadherin, α-smooth muscle actin (α-SMA), Vimentin and β-Actin. The autophagy was visualized by microtubule-associated protein 1A/1B-light chain 3 (LC3) staining and western blot.

Results: The results showed that cell proliferation was significantly inhibited and apoptotic and necrotic cells were significantly increased with 2 μM of erastin treatment. Western blotting showed that reactive oxygen species (ROS) production and the level of heme oxygenase-1 were increased in the cells. Epithelial-mesenchymal transition (EMT) represented by the suppression of E-cadherin and the upregulation of α-smooth muscle actin (α-SMA) and Vimentin was induced by erastin. Additionally, autophagy represented by activated LC3B and up-regulated Beclin-1 were also induced by erastin. To further ascertain the role of autophagy in erastin-induced EMT, chloroquine, which is an autophagy inhibitor, was employed, and was found to effectively reduce EMT in this process.

Conclusions: These results support the role of the enhanced accumulation of iron as a mechanism for increasing the vulnerability of lung epithelial cells to iron-driven oxidant injury that triggers further autophagy during EMT.

Keywords: Iron metabolism; ferroptosis; epithelial-mesenchymal transition (EMT); idiopathic pulmonary fibrosis (IPF)

Submitted Sep 14, 2021. Accepted for publication Dec 08, 2021.
doi: 10.21037/atm-21-5404
View this article at: https://dx.doi.org/10.21037/atm-21-5404

^ ORCID: 0000-0002-9792-5127.

Introduction

Idiopathic pulmonary fibrosis (IPF) is a refractory lung fibrotic disease pathologically characterized by epithelial injury, fibroblastic proliferation, and extracellular matrix deposition in the lung parenchymal (1). Treatment options for IPF are limited. Further, the progression of the disease can only be slowed and cannot be reversed by existing therapies.

Lung epithelial cells are considered a key player in the pathogenesis of IPF. Lipid peroxidation appears to be increased in IPF patients and is thought to be associated with increased deferoxamine-chelate iron levels (2). As recent research on alveolar epithelial cell apoptosis and underlying myofibroblasts in the lungs of patients has shown, epithelial-mesenchymal transition (EMT) and its intermediate states are vital drivers of organ fibrosis, including IPF (3). Myofibroblasts accumulate and secrete excessive collagen in fibrotic tissues, damaging organs and leading to organ failure.

Autophagy is a lysosomal-mediated catabolic pathway that eliminates unnecessary components, and thus maintains cellular viability and homeostasis. Intracellular substrates are sequestered into double-membraned autophagosomes, and are subsequently degraded after autophagosome-lysosome fusion during the process of autophagy. Selective autophagy that recycles specific components (e.g., ferritin) is generally considered a cellular response to stress. Ferroptosis, a novel form of regulated cell death, is characterized by the production of reactive oxygen species (ROS) from accumulated iron and lipid peroxidation (4). Iron is an essential element of growth and development that becomes toxic at high levels, and thus its metabolism is tightly controlled.

Iron metabolism is of crucial importance for the lungs. Iron deficiency might explain the mitochondrial suppression, metabolic changes, and proliferative and apoptosis-resistant signaling pathways identified in pulmonary arterial hypertension (5). Additionally, labile iron accumulation accompanies necrotic cell death during cigarette smoke exposure, which plays a vital role in the development of chronic obstructive pulmonary disease (6). Further, there are elevated concentrations of alveolar fluid and tissue iron in human lung allografts, which may increase the exposure risk of lung allografts to iron radicals, ROS, and subsequent fibrosis (7). Erastin is a small molecule capable of triggering ferroptosis, a described caspase-independent form of regulated necrosis characterized by an increase of detrimental intracellular ROS produced by iron-dependent lipid peroxidation (1).

Despite the accepted detrimental role of iron overload, the exact mechanism of how iron accumulation develops to IPF requires further investigation. In this study, we sought to assess the *in vitro* role of iron in the progression of fibrosis in lung epithelial cells and examine the possible regulation of iron and IPF. We present the following article in accordance with the MDAR reporting checklist (available at https://dx.doi.org/10.21037/atm-21-5404).

Methods

Cell culture

Mouse lung epithelial cell line 12 (MLE-12) cells (Cell Resource Center, Chinese Academy of Sciences, Shanghai, CN) were cultured in Dulbecco's Modified Eagle Medium/Nutrient Mixture F-12 (Gibco, Grand Island, NY, USA) supplemented with 5% heat-inactivated fetal bovine serum (Gibco, Grand Island, NY, USA) and incubated in a humidified atmosphere with 5% carbon dioxide at 37 ℃. Deoxyribonucleic acid (DNA) profiling was used to identify the cell line (of short tandem repeats), and mycoplasma contamination was tested using the Lonza MycoAlert Mycoplasma Detection Kit (LONZA, Rockland, ME, USA).

Cell Counting Kit-8 (CCK-8) assay

The MLE-12 cells were seeded in a 96-well plate at a density of 4×10^4 cells/well. After overnight culture, they were treated with or without 1 or 2 μM of erastin (Sigma, St. Louis, MO, USA) and incubated at 37 ℃ for another 24 hours. A total of 10 μL of CCK-8 reagent (Dojindo Laboratories, Tokyo, Japan) was used to measure cell viability.

RNA extraction and qPCR

Ribonucleic acid (RNA) was extracted from the MLE-12 cells using Trizol reagent (Invitrogen, Carlsbad, CA, USA) in accordance with the supplier's instructions. 1 μg of total RNA was reverse transcribed using the reverse transcription kit (Promega, Madison, WI, USA) with oligo(dT) primers. A SYBR Green (Toyobo, Osaka, Japan) stained quantitative polymerase chain reaction (qPCR) was conducted to analyze the expression of E-cadherin, N-cadherin, α-smooth muscle actin (α-SMA), and β-Actin (as an internal control) in

messenger RNA (mRNA). The following primers were used for E-cadherin: 5'-CTGGTGGAGAAGTATGGGCT-3' and 5'-AGGTTGTCCAGGGTGATGC-3'; N-cadherin: 5'-CGGTGATGCGGTATGAAGAG-3' and 5'-ATTCGGTCTGTGTCGGCTGCAT-3'; α-SMA: 5'-TGGATGGAGACAGTGAAGGTG-3', and 5'-CACGCACACCAAGCCAAACT-3'; β-Actin: 5'-GGATGGAAAGCGCAAGACAC-3' and 5'-ATGGCCATCAAAGTATCCCG-3'. mRNA expressions of the targeted gene were normalized to β-Actin mRNA expression, and the relative amounts of all mRNAs were calculated using the comparative Ct method.

Measurement of the intracellular iron level

The intracellular iron levels were measured with an iron assay kit according to the manufacturer's instructions (Abcam, Cambridge, MA, USA).

Western blot

The MLE-12 cells were harvested and centrifuged at 800 g for 5 minutes to pellet the cell debris. The cells were lysed in radioimmunoprecipitation assay buffer containing proteinase and phosphatase inhibitors. Protein concentrations were measured using the bicinchoninic acid protein assay kit (Pierce, Rockford, IL, USA). After sodium dodecyl sulphate-polyacrylamide gel electrophoresis, the proteins were transferred to polyvinylidene fluoride membranes (Millipore, Bedford, MA, USA) and blocked for 1 hour in non-fat milk, and then incubated in the primary antibody overnight at 4 ℃. After washing 3 times, the blots were incubated in infrared-dye-based secondary antibodies (LI-COR) for 1 hour at room temperature. Next, the antibody signals were detected using the Odyssey scanner (LI-COR Biosciences, Lincoln, NE, USA). The Western blot data were quantified through the densitometry of the bands using Odyssey analyzer software (LI-COR Biosciences, Lincoln, NE, USA). Rabbit anti-LC3-I, anti-LC3-II (1:500, Cell Signaling Technology, Beverly, MA, USA), mouse anti-E-cadherin (1:500, Cell Signaling Technology, Beverly, MA, USA), mouse anti-N-cadherin (1:500, Cell Signaling Technology, Beverly, MA, USA), rabbit anti-Beclin-1 (1:500, Cell Signaling Technology, Beverly, MA, USA), rabbit anti-α-SMA (1:500, Cell Signaling Technology, Beverly, MA, USA), rabbit anti-Vimentin (1:500, Cell Signaling Technology, Beverly, MA, USA), mouse anti-proliferating cell nuclear antigen (PCNA; 1:500, Sigma, St. Louis, MO, USA), rabbit anti-heme oxygenase-1 (HO-1; 1:500, Cell Signaling Technology, Beverly, MA, USA), and mouse anti-β-Actin (1:500, Sigma, St. Louis, MO, USA) were used as primary antibodies, and IR-dye based goat anti-mouse or goat anti-rabbit immunoglobulin G (1:10,000, LI-COR Biosciences, Lincoln, NE, USA) were use as secondary antibodies.

Cell death assay

The MLE-12 cells were seeded in a 96-well plate at a density of 4×10^4 cells/well. After overnight culture, they were treated with or without 2 μM of erastin (Sigma, St. Louis, MO, USA) and incubated at 37 ℃ for another 24 hours. The cell death assay was performed using an annexin V/propidium iodide (PI) fluorescence detection kit (BD Bioscience, Bedford, MA, USA). The images were taken by the Operetta high-content imaging system (PerkinElmer, Waltham, MA, USA) and analyzed by the Harmony software (PerkinElmer, Waltham, MA, USA).

Detection of autophagy

The MLE-12 cells were seeded in a 96-well plate at a density of 4×10^4 cells/well. After overnight culture, the cells were transducing autophagy tandem sensor GFP-LC3-II kit (Life Technologies, Carlsbad, CA, USA) following the manufacturer's protocol. After overnight culture, MLE-12 cells were treated with or without 2 μM of erastin (Sigma, St. Louis, MO, USA) and incubated at 37 ℃ for another 24 hours. Then images were taken using the Operetta high-content imaging system (PerkinElmer, Waltham, MA, USA) and analyzed using Harmony Software (PerkinElmer, Waltham, MA, USA).

Detection of ROS

The MLE-12 cells were seeded in a 96-well plate at a density of 4×10^4 cells/well. After overnight culture, they were treated with or without 2 μM of erastin (Sigma, St. Louis, MO, USA) and incubated at 37 ℃ for another 24 hours. Intracellular ROS were detected using CellROX® Reagent (Life Technologies, Carlsbad, CA, USA).

Statistical analysis

The experiments were repeated at least 3 times each. The data are expressed as means ± standard error of the mean.

The statistical analyses were performed using a 2-tailed unpaired *t*-test for two groups and a One-way analysis of variance with a post-hoc test for multiple groups using Prism5 (GraphPad Software, La Jolla, CA). A P value <0.05 was considered statistically significant.

Results

Erastin inhibited cell proliferation in MLE-12 cells

The MLE-12 cells were exposed to two different concentrations of erastin (i.e., 1 or 2 μM) for 24 hours. The CCK8 was used for the proliferation assay, and the results showed that 2 μM of erastin decreased cell proliferation by around 10% in the incubated MLE-12 cells, while 1 μM of erastin slightly increased cell proliferation (see *Figure 1A,1B*). Additionally, the expression of PCNA, a standard cell proliferation marker, which regulated DNA replication, was inhibited by 2 μM of erastin. Conversely, expression was upregulated in the cells incubated with 1 μM of erastin (see *Figure 1C,1D*). Cell death was also measured by annexin V staining. Cell populations with annexin V–/PI–, annexin V+/PI–, annexin V–/PI+ and annexin V+/PI+ were regarded as live cells, early apoptotic, necrotic and late apoptotic cells, respectively. The results showed that the number of cell death (including apoptotic and necrotic cells) significantly increased in cells treated with 2 μM of erastin compared to cells treated without erastin, nevertheless, the total percentage of 2 μM of erastin-induced cell death was no more than 15%, which indicated that 2 μM of erastin had minor effect on cell death (see *Figure 1E-1H*).

Erastin increased cytoplasmic oxidative stress in MLE-12 cells

Based on the above-mentioned findings, 2 μM was considered the appropriate concentration for erastin in the subsequent experiments. We found the serum ferric and ferrous iron were both remarkably upregulated in cells treated with 2 μM of erastin (see *Figure 2*) as was ROS production (see *Figure 3A,3B*). To further examine the effect of erastin incubation on antioxidant enzymes, we quantified the heme oxygenase-1 (HO-1) levels in the MLE-12 cells, and observed more than a 2-fold increase (see *Figure 3C,3D*). Thus, erastin increased cytoplasmic oxidative stress in MLE-12 cells.

Erastin treatment induced autophagic flux in MLE-12 cells

We transfected the MLE-12 cells with tandem fluorescent mRFP-GFP-LC3II, a novel marker assessing autophagic flux. The autophagosomes were processed after being fused with lysosomes using fluorescence microscopy. Erastin increased red puncta more than 5-fold in the merged images, indicating autolysosome formation (see *Figure 4A,4B*). We also examined the processing of full-length LC3-I to LC3-II, which is a hallmark of autophagy, in the erastin-treated MLE-12 cells. Erastin exposure increased the protein levels of LC3-II but decreased the levels of LC3-I, which in turn led to a decrease in the LC3-I/LC3-II ratio (see *Figure 4C,4D*). Further, Beclin-1, which is 1 of the first mammalian autophagy effectors to be identified, was 1-fold upregulated in the MLE-12 cells treated with erastin (see *Figure 4C,4E*). Thus, erastin treatment induced autophagic flux in the MLE-12 cells.

Autophagy functioned as a promotor in erastin-induced EMT in MLE-12 cells

To directly examine whether erastin could induce EMT, 2 approaches were adopted to evaluate E-cadherin, which is a characteristic epithelial marker, expression in the MLE-12 cells after erastin incubation. The quantitative reverse transcription (qRT)-PCR analysis revealed the transient suppression of E-cadherin mRNA levels (see *Figure 5A*). A quantitative immunoblot analysis of the protein extracted from the MLE-12 cells revealed a comparable reduction in E-cadherin protein content (see *Figure 5B,5C*). Further, in cells undergoing EMT, the loss of epithelial markers was accompanied by mesenchymal characteristics. Thus, we used equally rigorous approaches to determine whether MLE-12 cells upregulated mesenchymal genes after erastin treatment. α-SMA and Vimentin are two main markers of myofibroblasts, smooth muscle cells, cells originated from mesenchymal and EMT occurrence. The results of the qRT-PCR and western blot analysis confirmed that the MLE-12 cells upregulated the expression of α-SMA and Vimentin (see *Figure 5B,5D-5G*). However, there was no change of N-cadherin mRNA and protein expression in cells treated with 2 μM of erastin (see *Figure 5B,5H,5I*).

To further ascertain the role of autophagy in erastin-induced EMT, chloroquine (CQ), which is an autophagy inhibitor, was employed. As *Figure 6* shows, CQ (50 μM)

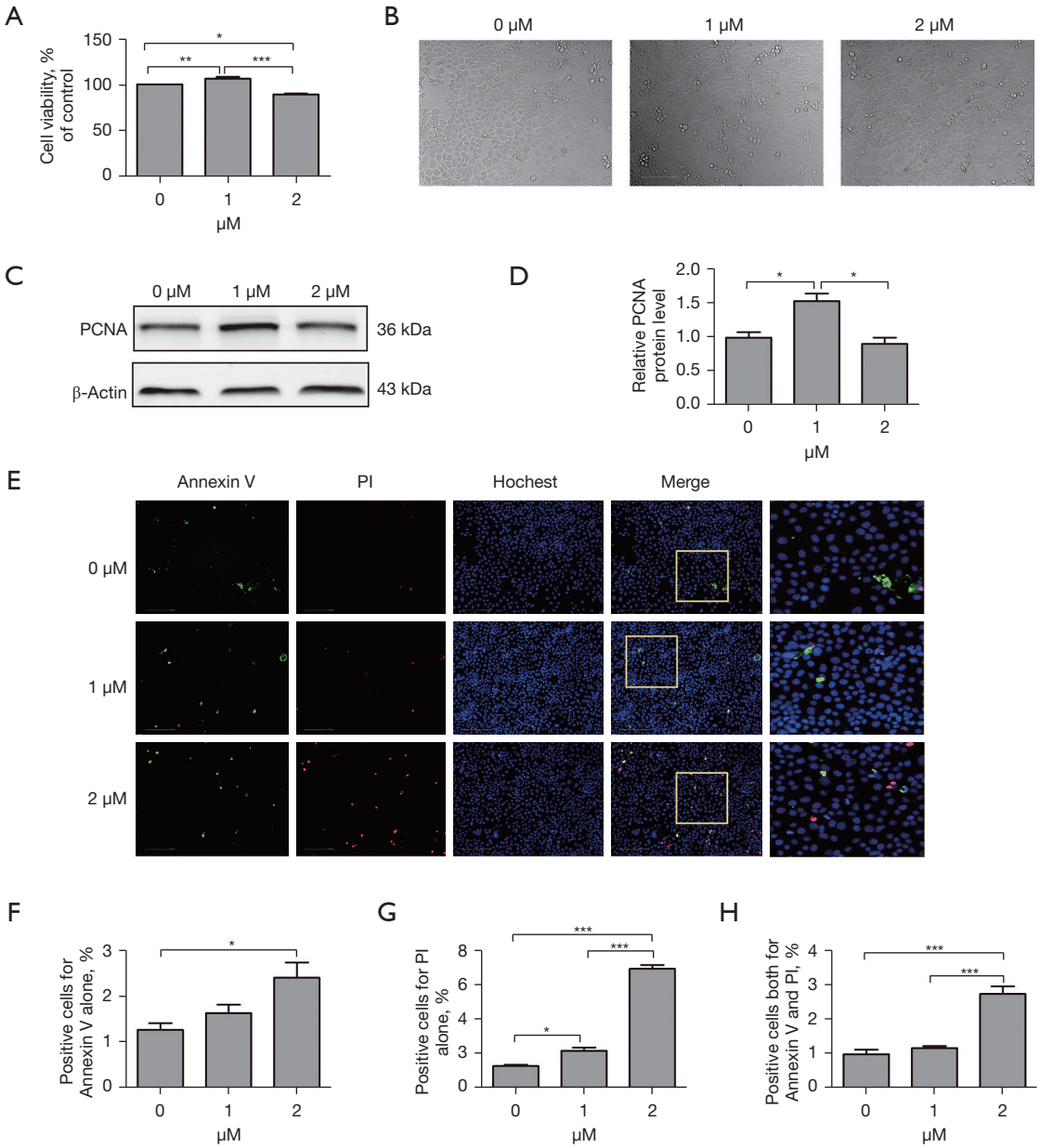

Figure 1 Erastin inhibited cell proliferation in Mouse lung epithelial cell line 12 (MLE-12) cells. (A) The quantification of cell viability in MLE-12 cells exposed to erastin (for 24 hours). The average quantification of MLE-12 cells after 24 hours of exposure to erastin was counted in 5 randomly chosen fields. (B) The representative images of proliferation in erastin-induced MLE-12 cells (scale bar: 100 μm). (C,D) A Western blot analysis of proliferating cell nuclear antigen (PCNA) expression in MLE-12 cells after 24 hours of exposure to erastin. β-actin was used as a loading control. (E) Cell death after erastin exposure was measured by annexin V (apoptotic cells), propidium iodide (PI, dead cells), and Hochest33342 (nuclei) staining (×400). (F-H) The quantification of annexin V and PI fractions showed that induced-cell death was significantly higher in cells with a high concentration of erastin than in control cells. All data are presented as mean ± standard deviation. *, P<0.05; **, P<0.01; ***, P<0.001. Experiments were performed in triplicate.

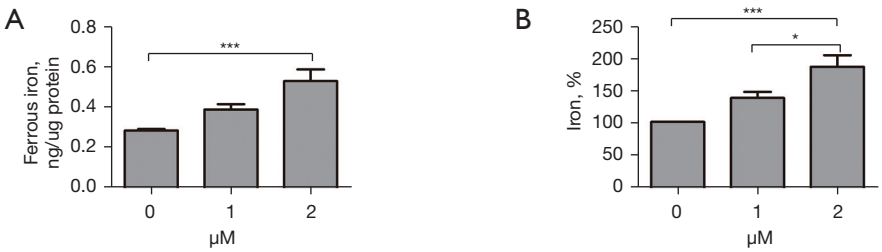

Figure 2 Eastin increased iron accumulation in MLE-12 cells. (A,B) The quantification of intracellular ferrous and ferric iron levels was measured with an iron assay kit. The intracellular iron levels were significantly increased in the erastin-induced MLE-12 cells with higher concentrations. All data are presented as mean ± standard deviation. *, P<0.05; ***, P<0.001. Experiments were performed in triplicate.

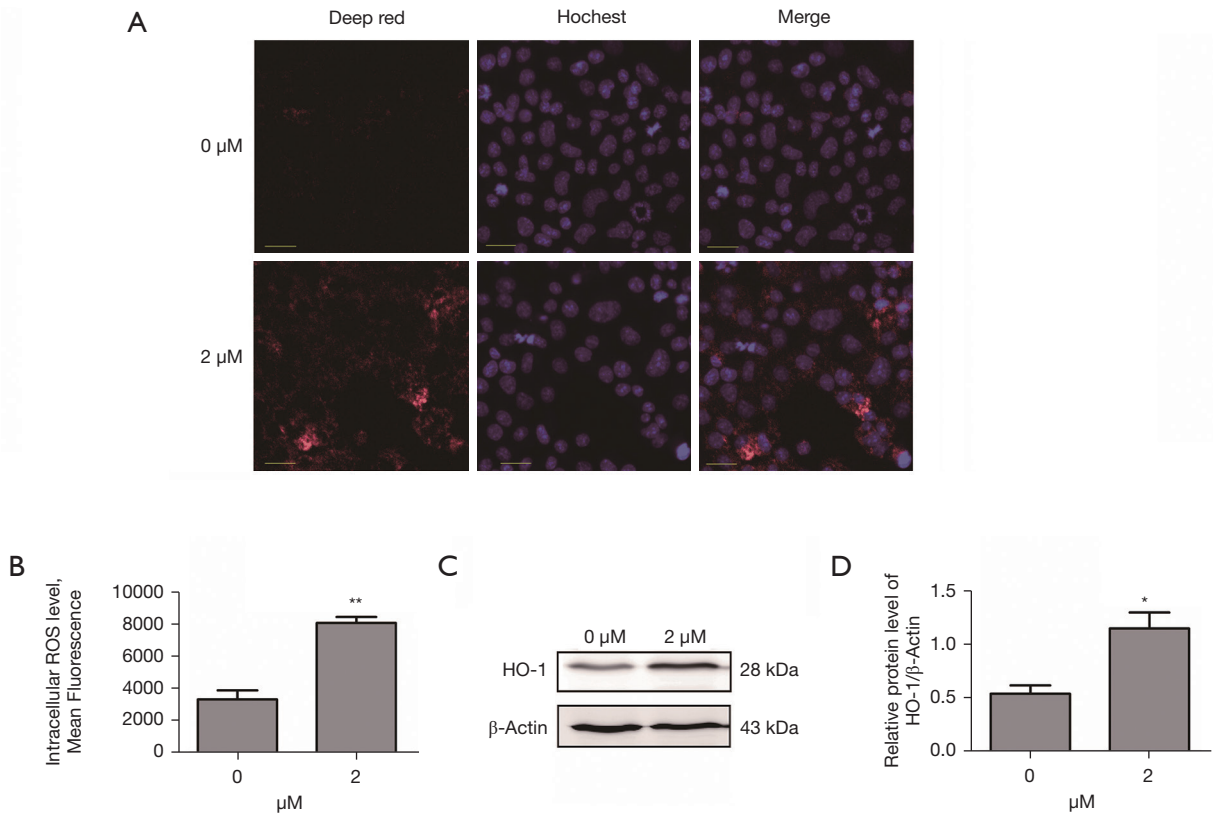

Figure 3 Erastin increased cytoplasmic oxidative stress in MLE-12 cells. (A) Immunofluorescent analysis of reactive oxygen species (ROS) in MLE-12 cells with or without erastin incubation for 24 hours. The density of red fluorescence indicates the ROS level (scale bar: 50 μm). (B) Changes in ROS production in MLE-12 cells are presented as a red fluorescence ratio. (C) A Western blot analysis showing that the MLE-12 cells incubated with 2 μM of erastin showed increased heme oxygenase-1 (HO-1) expression. (D) The ratio of HO-1/β-actin in the MLE-12 cells under the control and erastin conditions. β-actin was used as a loading control. All data are presented as mean ± standard deviation. *, P<0.05; **, P<0.01. Experiments were performed in triplicate.

reduced the percentage of autophagy (the LC3-I/LC3-II ratio) and α-SMA by nearly 4-fold, and increased E-cadherin 2-fold (see *Figure 6A-6D*), which indicated that EMT was reduced in the MLE-12 cells. Additionally, the mRNA level of collagen I, which is a fibrosis marker, was reduced by nearly 30% by the CQ treatment (see *Figure 6E*). Thus, we concluded that erastin functioned as a promotor in EMT and of fibrogenesis in MLE-12 cells.

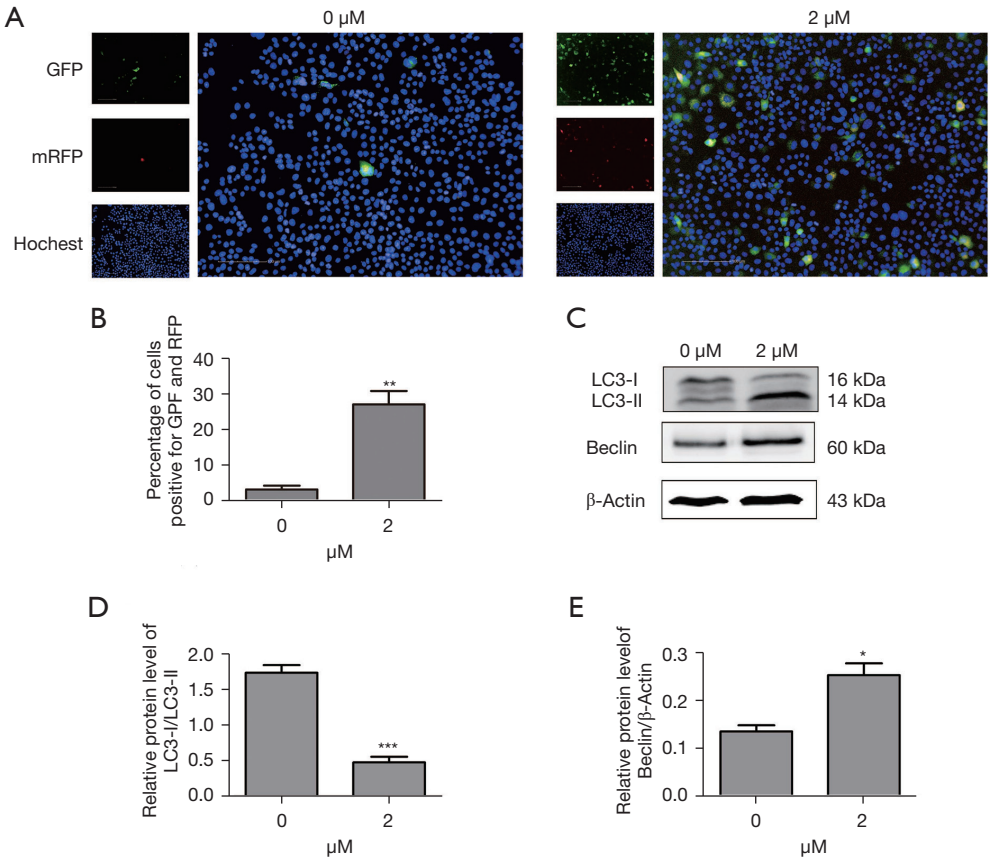

Figure 4 Erastin promoted autophagy in MLE-12 cells. (A) Immunofluorescent images of MLE-12 cells transfected with plasmids encoding mRFP-GFP-LC3II and treated with or without 2 μM of erastin for 24 hours. The density of red fluorescence indicates the LC3-II level. (B) Changes in the autophagy flux of the erastin-treated MLE-12 cells were measured as mRFP-GFP-LC3II/Hochest. (C) Representative immunoblots depicting levels of LC3-I, LC3-II, and Beclin-1 using their respective antibodies. β-actin was employed as the loading control. (D) The ratio of LC3-I/LC3-II in the MLE-12 cells under the control and erastin conditions. (E) The quantification of the relative protein expression of Beclin-1 was determined by a densitometric analysis; β-actin was used as a loading control. All data are presented as mean ± standard deviation. *, P<0.05; **, P<0.01; ***, P<0.001. Experiments were performed in triplicate.

Discussion

Lung epithelial cells are considered a key player in IPF pathogenesis. Patients with IPF have been found to have increased deferoxamine-chelate iron levels (2). Iron is required for normal cellular functions; however, inappropriately high concentrations of iron may be lethal. Thus, lung epithelial cells must efficiently sequester and process excessive iron without inappropriate activation. Our data indicated an increase of cytoplasmic oxidative stress induced by the expansion of serum ferric and ferrous iron, which then activated autophagy and the expression of profibrotic factors, leading to EMT.

Erastin, which is a Ras selective lethal compound (8), is a small molecule capable of triggering ferroptosis, a described caspase-independent form of regulated necrosis characterized by an increase of detrimental intracellular ROS produced by iron-dependent lipid peroxidation (1). Dysregulated ferroptosis has been implicated in several physiological and pathological processes, including cancer cell death, tissue injury, and T-cell immunity (4). The present study appears to be the first to examine the role of iron-driven oxidative damage in EMT. Similar to a previous study of other diseases (8), this study showed that erastin-stimulated MLE-12 cells cultured *in vitro* had an overload of iron and cytoplasmic oxidative stress and increased cell death (see *Figures 1-3*).

We also transfected MLE-12 cells with tandem

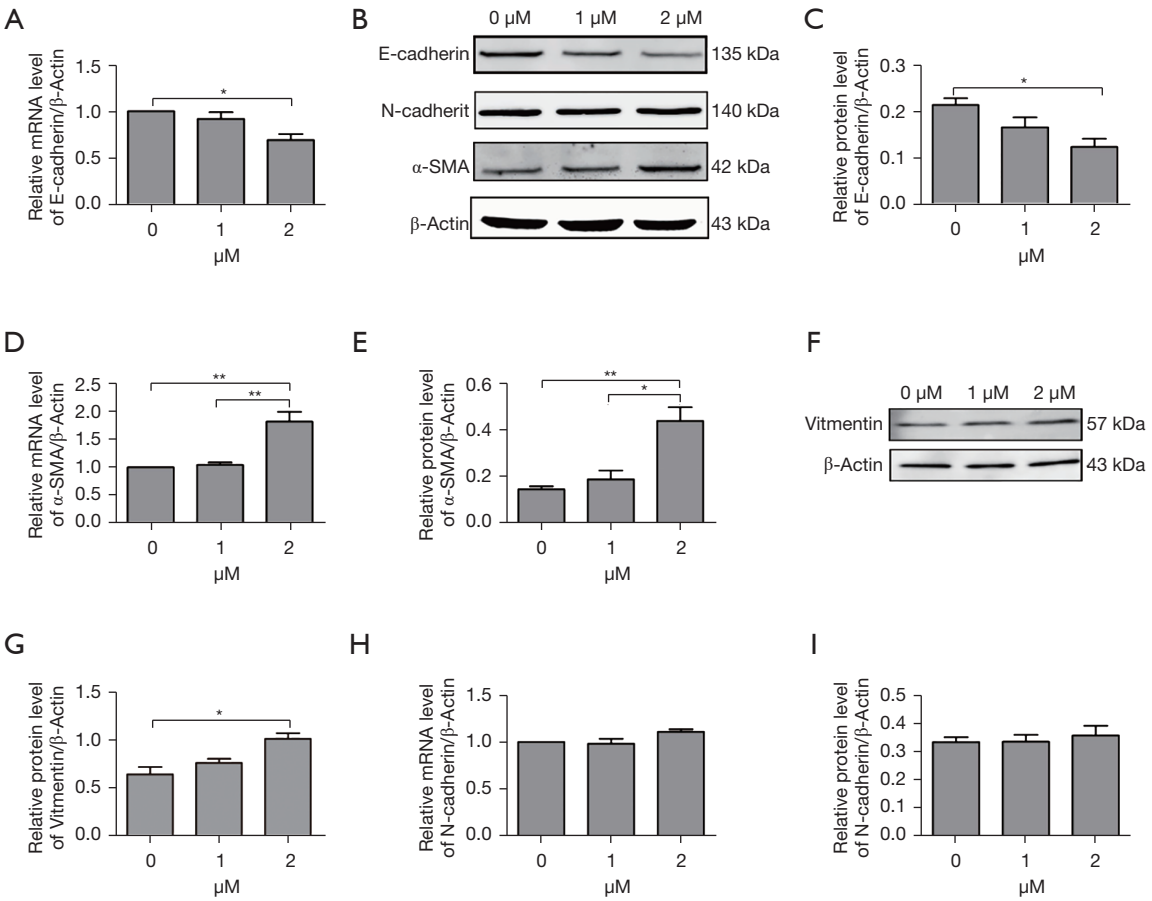

Figure 5 Erastin functioned as a promotor in epithelial-mesenchymal transition (EMT) and of fibrogenesis in MLE-12 cells. (A) The quantitative polymerase chain reaction (qPCR) evaluation of mRNA expression of E-cadherin in MLE-12 cells exposed to different concentrations of erastin. (B) Representative immunoblots depicting protein levels of E-cadherin, N-cadherin and α-SMA using their respective antibodies. β-actin was used as the internal control. (C) The protein ratio of E-cadherin/β-actin in MLE-12 cells exposed to different concentrations of erastin. (D,E) The qPCR evaluation of mRNA expression and protein ratio of α-SMA. (F,G) Immunoblots depicting protein levels of Vimentin and protein ratio quantitative analysis of Vimentin/β-actin. (H,I) The qPCR evaluation of mRNA expression and protein ratio of N-cadherin. *, P<0.05; **, P<0.01.

fluorescent mRFP-GFP-LC3B, a novel marker, to assess autophagic flux, and found that erastin increased the formation of autolysosomes, and increased the protein levels of LC3-II, but decreased the levels of LC3-I, and Beclin-1, which was 1 of the first mammalian autophagy effectors identified. Thus, we found that erastin treatment induced autophagic flux in the MLE-12 cells (see *Figure 4*).

Autophagy is a natural, regulated, and destructive biological process that disassembles unnecessary or dysfunctional cell components. The core machinery of autophagy consists of over 30 autophagy-related proteins, including Beclin-1 and LC3-II. Beclin-1 is an autophagosome initiation protein, which has been shown to promote autophagy, suppress mammalian target of rapamycin signaling, improve cardiac function, and alleviate inflammation and fibrosis after a lipopolysaccharide (LPS) challenge (9). LC3-II is a structural component of autophagosomes (10). Iron triggers oxidative damage to lysosomal membranes, resulting in lysosomal leakage under oxidative stress (11).

As a consequence of activated autophagy, cells become trapped in a self-perpetuating cycle, promoting other types of autophagy. Unless the poisonous circle is broken, it leads to inflammation, cell death, tissue damage, and fibrosis (12). Thus, autophagy can be induced by the ferroptosis inducer, erastin, triggered by erastin-induced ROS, and inhibited by

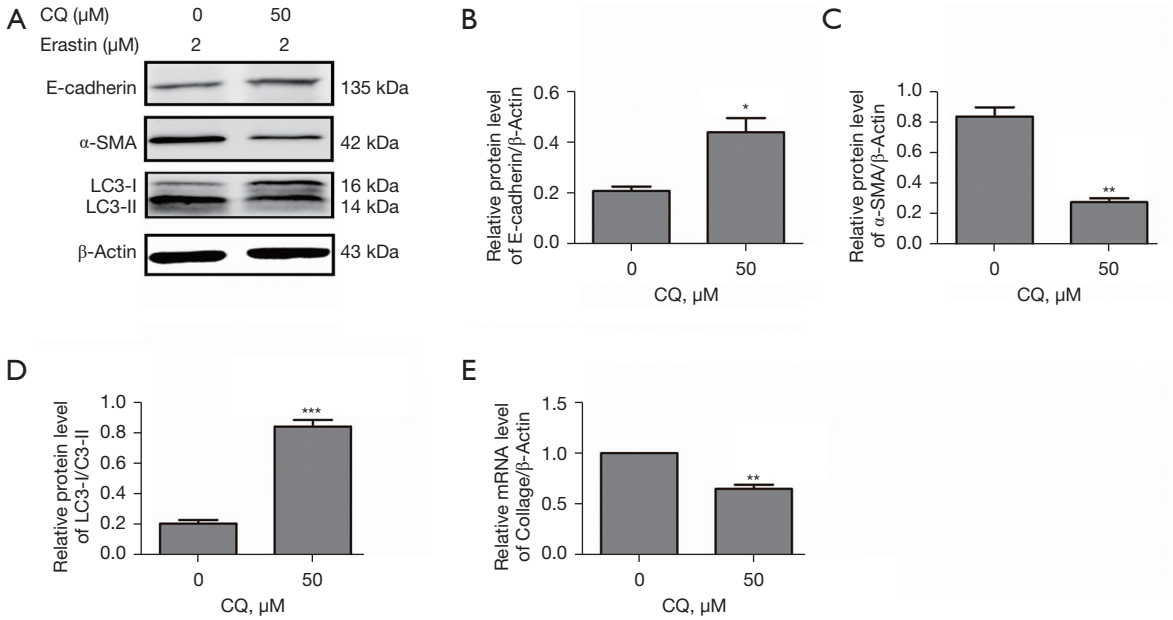

Figure 6 Autophagy was involved in the regulation of erastin-induced EMT in MLE-12 cells. (A) Representative immunoblots depicting levels of E-cadherin, α-SMA, and LC3-I/LC3-II in MLE-12 cells exposed to erastin (24 hours) with or without chloroquine (CQ) treatment. β-actin was used as the loading control. (B-D) The quantification of the relative protein expressions of E-cadherin, α-SMA, and LC3-I/LC3-II was determined by a densitometric analysis, which showed that the LC3-I/LC3-II ratio increased, E-cadherin increased, and α-SMA decreased with CQ treatment. (E) The qPCR evaluation of collagen I messenger ribonucleic acid (mRNA) performed in MLE-12 cells with or without CQ suggested reduced collagen I expression with CQ treatment. Experiments were performed in triplicate. *, P<0.05; **, P<0.01; ***, P<0.001.

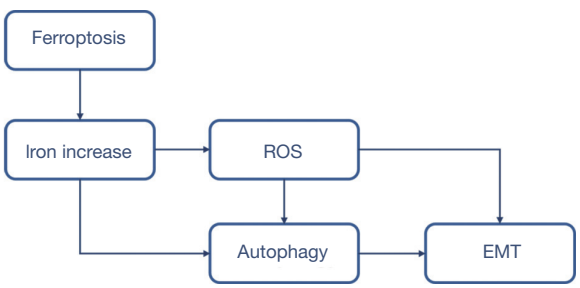

Figure 7 A diagram depicting the pathway in which intracellular iron, oxidative stress, autophagy, and EMT modulate pulmonary fibrosis. EMT, epithelial-mesenchymal transition.

ROS scavengers (13). Autophagy also promotes ferroptosis by degrading ferritin (14).

EMT is believed to be a mechanism of end-stage fibrosis, which is found in various interstitial lung diseases (11). To examine whether erastin could induce EMT, we evaluated E-cadherin, the characteristic epithelial marker. We observed that erastin suppressed E-cadherin and upregulated α-SMA. However, no changes in N-cadherin were observed (see *Figure 5*). Conversely, CQ treatment reduced α-SMA and collagen I, and increased E-cadherin, which led to reduced EMT and fibrosis in the MLE-12 cells (see *Figure 6*). CQ raised the pH inside cells and blocked the fusion of lysosomes with autophagosomes, which in turn reduced the activity of the lysosomal enzymes. It was also the most efficient compound at preventing EMT (see *Figure 7*). Thus, erastin appears to function as a promotor in EMT and fibrogenesis in MLE-12 cells, and autophagy inhibitors might serve as a potential therapeutic target for IPF.

Researchers have showed that autophagy, which acts as a significant regulator of cellular homeostasis by degrading damaged proteins and cytoplasmic components, is involved in EMT (15). However, the relationship between autophagy and EMT has not been fully explored. Autophagy and EMT markers were reported as additional prognostic indicators for patients' overall survival with cancers (16). Gugnoni found that cadherin-6 promoted EMT and cancer metastasis by restraining autophagy (17). Lai *et al.* showed that hypoxia-inducible factor-1α promoted autophagic proteolysis and

facilitated EMT and metastasis in mice (18). Han *et al.* found that Sirtuin 6 regulated the EMT of hepatocellular carcinoma by stimulating the autophagic degradation of E-cadherin (19). Studies have also shown that generated ROS and autophagosome formation lead to EMT, which is further promoted by the additional ROS-generating cytokine. These findings provide further evidence that the enhanced autophagic degradation of ferritin is a mechanism of autophagy triggering that increases the vulnerability of lysosomes to iron-driven oxidant injury during EMT (11,13,20,21).

In our study, the activated EMT (induced by ferroptosis) in the MLE-12 cells was successfully stopped by an inhibitor of autophagy, which confirmed our hypothesis that iron accumulates play a vital role in the pathogenesis of IPF. Thus, we concluded that ferroptosis functioned as a promotor in EMT and fibrogenesis in MLE-12 cells. Further, our results also suggest that autophagy inhibitors might be a potential therapeutic target for IPF.

Conclusions

The present study provides further evidence that enhanced iron accumulation is a mechanism for increasing the vulnerability of the lung epithelial cells to iron-driven oxidant injury that triggers further autophagy during EMT. These findings provide novel insights into potential therapeutic targets for IPF patients.

Acknowledgments

Funding: This work was supported by funding from the National Natural Science Foundation of China (81400043), the Shanghai Municipal Key Clinical Specialty (shslczdzk02201), the Shanghai Top-Priority Clinical Key Disciplines Construction Project (2017ZZ02013) and the Shanghai Pujiang Program (2020PJD011).

Footnote

Reporting Checklist: The authors have completed the MDAR checklist. Available at https://dx.doi.org/10.21037/atm-21-5404

Data Sharing Statement: Available at https://dx.doi.org/10.21037/atm-21-5404

Conflicts of Interest: All authors have completed the ICMJE uniform disclosure form (available at https://dx.doi.org/10.21037/atm-21-5404). The authors have no conflicts of interest to declare.

Ethical Statement: The authors are accountable for all aspects of the work in ensuring that questions related to the accuracy or integrity of any part of the work are appropriately investigated and resolved.

References

1. Minagawa S, Yoshida M, Araya J, et al. Regulated Necrosis in Pulmonary Disease. A Focus on Necroptosis and Ferroptosis. Am J Respir Cell Mol Biol 2020;62:554-62.
2. Jack CI, Jackson MJ, Johnston ID, et al. Serum indicators of free radical activity in idiopathic pulmonary fibrosis. Am J Respir Crit Care Med 1996;153:1918-23.
3. Nieto MA, Huang RY, Jackson RA, et al. EMT: 2016. Cell 2016;166:21-45.
4. Xie Y, Hou W, Song X, et al. Ferroptosis: process and function. Cell Death Differ 2016;23:369-79.
5. Sutendra G, Bonnet S. The iron paradigm of pulmonary arterial hypertension: Popeye knows best. Circ Res 2015;116:1636-8.
6. Ghio AJ, Hilborn ED, Stonehuerner JG, et al. Particulate matter in cigarette smoke alters iron homeostasis to produce a biological effect. Am J Respir Crit Care Med 2008;178:1130-8.
7. Baz MA, Ghio AJ, Roggli VL, et al. Iron accumulation in lung allografts after transplantation. Chest 1997;112:435-9.
8. Dixon SJ, Lemberg KM, Lamprecht MR, et al. Ferroptosis: an iron-dependent form of nonapoptotic cell death. Cell 2012;149:1060-72.
9. Sun Y, Yao X, Zhang QJ, et al. Beclin-1-Dependent Autophagy Protects the Heart During Sepsis. Circulation 2018;138:2247-62.
10. Zhao H, Chen H, Xiaoyin M, et al. Autophagy Activation Improves Lung Injury and Inflammation in Sepsis.

Inflammation 2019;42:426-39.
11. Sioutas A, Vainikka LK, Kentson M, et al. Oxidant-induced autophagy and ferritin degradation contribute to epithelial-mesenchymal transition through lysosomal iron. J Inflamm Res 2017;10:29-39.
12. Linder MC. Mobilization of stored iron in mammals: a review. Nutrients 2013;5:4022-50.
13. Park E, Chung SW. ROS-mediated autophagy increases intracellular iron levels and ferroptosis by ferritin and transferrin receptor regulation. Cell Death Dis 2019;10:822.
14. Hou W, Xie Y, Song X, et al. Autophagy promotes ferroptosis by degradation of ferritin. Autophagy 2016;12:1425-8.
15. Akalay I, Janji B, Hasmim M, et al. Epithelial-to-mesenchymal transition and autophagy induction in breast carcinoma promote escape from T-cell-mediated lysis. Cancer Res 2013;73:2418-27.
16. Wang JY, Wu T, Ma W, et al. Expression and clinical significance of autophagic protein LC3B and EMT markers in gastric cancer. Cancer Manag Res 2018;10:1479-86.
17. Gugnoni M, Sancisi V, Gandolfi G, et al. Cadherin-6 promotes EMT and cancer metastasis by restraining autophagy. Oncogene 2017;36:667-77.
18. Lai HH, Li JN, Wang MY, et al. HIF-1α promotes autophagic proteolysis of Dicer and enhances tumor metastasis. J Clin Invest 2018;128:625-43.
19. Han LL, Jia L, Wu F, et al. Sirtuin6 (SIRT6) Promotes the EMT of Hepatocellular Carcinoma by Stimulating Autophagic Degradation of E-Cadherin. Mol Cancer Res 2019;17:2267-80.
20. Radisky DC, Levy DD, Littlepage LE, et al. Rac1b and reactive oxygen species mediate MMP-3-induced EMT and genomic instability. Nature 2005;436:123-7.
21. Schieber MS, Chandel NS. ROS links glucose metabolism to breast cancer stem cell and EMT phenotype. Cancer Cell 2013;23:265-7.

Cite this article as: Han Y, Ye L, Du F, Ye M, Li C, Zhu X, Wang Q, Jiang H, Liu Z, Ma J, Zhou J, Bai C, Song Y, Liu J. Iron metabolism regulation of epithelial-mesenchymal transition in idiopathic pulmonary fibrosis. Ann Transl Med 2021;9(24):1755. doi: 10.21037/atm-21-5404

